Signal Processing: Image Communication 68 (2018) 193–206

Contents lists available at ScienceDirect

Signal Processing: Image Communication

journal homepage: www.elsevier.com/locate/image

Holographic representation: Hologram plane vs. object plane

Marco V. Bernardo [a,*], Pedro Fernandes [a], Angelo Arrifano [a], Marc Antonini [b], Elsa Fonseca [c], Paulo T. Fiadeiro [d], António M.G. Pinheiro [a], Manuela Pereira [a]

[a] Instituto de Telecomunicações and Universidade da Beira Interior, Portugal
[b] I3S-CNRS, France
[c] Physics Department, Universidade da Beira Interior, Portugal
[d] Fiber Materials and Environmental Technologies (FibEnTech), Universidade da Beira Interior, Portugal

ARTICLE INFO

Keywords:
Digital holography
HEVC codec
Numerical reconstruction of holograms
Hologram plane
Object plane

ABSTRACT

Digital holography allows the recording, storage and subsequent reconstruction of both amplitude and phase of the light field scattered by an object. This is accomplished by recording interference patterns that preserve the properties of the original object field essential for 3D visualization, the so-called holograms.

Digital holography refers to the acquisition of holograms with a digital sensor, typically a CCD or a CMOS camera, and to the reconstruction of the 3D object field using numerical methods.

In the current work, the different representations of digital holographic information in the hologram and in the object planes are studied. The coding performance of the different complex field representations, notably Amplitude-Phase and Real-Imaginary, in both the hologram plane and the object plane, is assessed using both computer generated and experimental holograms. The HEVC intra main coding profile is used for the compression of the different representations in both planes, either for experimental holograms or computer generated holograms.

The HEVC intra compression in the object plane outperforms encoding in the hologram plane. Furthermore, encoding computer generated holograms in the object plane has a larger benefit than the same encoding over the experimental holograms. This difference was expected, since experimental holograms are affected by a larger negative influence of speckle noise, resulting in a loss of compression efficiency.

This work emphasizes the possibility of holographic coding on the object plane, instead of the common encoding in the hologram plane approach. Moreover, this possibility allows direct visualization of the Object Plane Amplitude in a regular 2D display without any transformation methods. The complementary phase information can easily be used to render 3D features such as depth map, multi-view or even holographic interference patterns for further 3D visualization depending on the display technology.

1. Introduction

Holography provides the possibility to fully reconstruct a complex wavefield by recording its interference with a coherent reference beam. It was first presented by D. Gabor in 1948 while trying to improve electron microscopy [1]. Shortly after the invention of Light Amplification by Stimulated Emission of Radiation (LASER), E. Leith and Upatnieks developed the first transmission hologram in 1962 [2,3], while Y. Denisyuk developed the first reflection hologram [4]. Traditionally, a hologram is an interference fringe pattern that is recorded in a photosensitive film using an appropriate optical setup. When that pattern is illuminated with the reference light, the diffracted wavefield fully reconstructs the captured object field along with all its properties: light intensity, parallax, and depth. In theory, there is no optical difference between the original and reconstructed object field.

Those earlier works lead in a short time to the production of the first Computer Generated Hologram (CGH). Lohmann and Paris made that breakthrough in 1967 using the limited computing capabilities at that time [5]. In 1980, Yaroslavskii and Merzlyakov established the theoretical background for CGH [6]. A digital hologram differs from a CGH in the sense that the generation of the interference patterns is performed optically instead of being artificially generated by numerical means. After Goodman and Lawrence [7] studies, digital holography development was followed by Kronrod et al. [8] who digitized optically enlarged parts of in-line and Fourier holograms to obtain numerical

* Corresponding author.
E-mail address: mbernardo@ubi.pt (M.V. Bernardo).

https://doi.org/10.1016/j.image.2018.08.006
Received 31 January 2018; Received in revised form 20 July 2018; Accepted 9 August 2018
Available online 23 August 2018

reconstructions of the original object fields. Later on, Onural and Scott made significant improvements in reconstruction algorithms [9,10]. However, a major step in digital holography occurred in the 1990's, when full digital recording and processing was made possible with the development of the first Charged Coupled Device (CCD). Schnars and Juptner presented the first direct recording of Fresnel holograms using this technique [11].

The referred advances in holography defined an important research topic, which is making its way into the most diverse applications including data storage [12–14], security [15,16], medical imaging [17,18], deformation/displacement measurement [19], and inevitably 3D displays [20,21]. Holographic 3D displays are certainly a promising technology, which found their interest in early Hollywood sci-fi movies. Currently, most advanced prototypes, the so-called light-field or holographic displays, can already display holographic information in full 3D, despite the limited resolution, and viewing angle.

1.1. Existing literature on holography coding

The first proposal for digital hologram coding and transmission dates from 1991, when Sato et al. [22] captured the holographic fringes using a camera, which was then modulated into a TV signal and transmitted to the receiver. In 1993, Yoshikawa realized that it is impractical to apply 2D image compression directly to the hologram. Instead, he proposes compressing hologram segments that correspond to different reconstruction perspectives. The segments were compressed with MPEG-1 and MPEG-2 [23,24]. In 2002, Naughton et al., studied the compressibility of phase-shifting digital holography using several lossless compression algorithms [25]. They concluded that better compression rates might be expected when the digital hologram is stored in an intermediate coding of separate data streams for real and imaginary components. Lossy compression techniques such as subsampling and quantization were also applied in [25]. Quantization proved to be a very effective technique. The effectiveness of quantization in both numerical simulation and optical experiments was confirmed by Mills and Yamaguchi [26]. The quantization on reconstruction domain of phase shifting holograms was analyzed by Darakis and Soraghan [27]. Naughton et al. in 2003 and Darakis et al. in 2006, demonstrated that the direct application of standard wavelets to holograms is not very efficient, since standard wavelets are typically designed to process piecewise smooth signals [28–30]. These authors proposed the use of a family of wavelet bases, named Fresnelets. Fresnelets were also applied in 2003 by Libeling et al. [31]. A similar study to [25] was provided by Frauel [32]. In 2006, Seo et al. proposed compressing hologram segments using multi-view and temporal prediction within a modified MPEG-2 [33,34]. Mills and I. Yamaguchi [26], Seo et al. [35], and Shortt et al., 2007 [36], considered the improvement of quantization of Real-Imaginary information. In 2010, Darakis et al. [37] determined the highest compression ratio that can be achieved on holograms while maintaining reconstruction quality at visually lossless levels. They used both MPEG-4 AVC and Dirac in their experiments. Based on scalar quantization, a multiple description coding method was applied to Amplitude-Phase information using maximum-a-posteriori [38]. It turned out to be a powerful mechanism to mitigate channel errors on digital holograms.

Complementary to the extensive studies on the performance of lossless coding and quantization methods, work on holographic data compression focused on lossy compression with wavelets transform were proposed. In 2013, Blinder et al. [39] investigated alternative wavelet decomposition on off-axis holograms. In 2014, Viswanathan et al. [40] used Morlet wavelets for transforming a hologram, and in 2015, Xing et al. [41] combined wavelet transform and joint encoding methods to compress phase-shifting holographic data.

In 2014, Still, Xing and Dufaux studied lossy coding based on scalar and vector quantization [42]. The same authors proposed a vector lifting scheme that exploits mutual redundancy [43].

More recently, Peixeiro et al. [44] performed a benchmark of the main available image coding standard solutions for digital holographic data, along with the main alternative representation formats. The standard image codecs: JPEG, JPEG 2000, H.264/AVC intra, HEVC intra main coding profile were compared. The authors concluded that the HEVC intra main coding profile is the best standardized coding solution and that the best representation formats are the Phase-Shifted Distances and Real-Imaginary.

Also in 2016, Dufaux et al. [45,46] reviewed the state of the art of the compression of digital holographic data. Several research lines were proposed by the authors, from which we point out the following three: the need for common datasets for a fair comparison of the proposed compression methods; the pursuit of better performance assessment methodologies; and finally, the urge to understand at which stage of the processing pipeline compression needs to be performed. This paper gives some contributions to these three points raised by Dufaux [46].

1.2. Main contributions

The first contribution of this paper is a database available online,[1] named EmergImg-HoloGrail, containing several sets of four interference patterns acquired in "Universidade da Beira Interior", by the phase shifting holography technique [47]. The sets of four phase-shifted holograms that are used to generate holograms can be found in the database. The Matlab codes for algebraic combination and numerical reconstruction of the interference patterns are also made available.

The second contribution is related with the choice of the compression plane. As presented above, several coding methods were used to study the characteristics of different representations. In the previous studies, the compression has been mostly applied to the hologram plane. Darakis and Soraghan [27] consider the compression on the object plane. These authors compare the quantization of the complex amplitudes on camera plane versus the quantization of complex amplitudes on the reconstruction plane. A single object acquired hologram and the normalized root-mean-square (NMRS) error for comparison, were used. They shown that the compression on reconstruction plane outperforms the compression on camera plane [27]. Furthermore, the application of Fresnelets can be understood as using a B-spline wavelet transform on the object plane. The Fresnelets coefficients are compressed more efficiently than the corresponding wavefront, since they reveal a higher spatially correlation [30]. In [30] the SPIHT coding of Fresnelets was proposed. They used the proposed method to compress one hologram representing a die. In the current study a similar analysis is overtaken. However, the Amplitude-Phase and Real-Imaginary representations are considered and coded independently. Moreover, the HEVC intra main coding profile is used since it was considered the best standardized coding solution for both hologram plane [44] and object plane [48]. Furthermore, experimental holograms and CGHs are considered in this study. Some of the holograms have multiple objects.

Finally, as last contribution, the quality was assessed in both hologram and object planes. Usually, reconstruction of the object is performed for quality assessment. However, as both planes were considered for quality assessment, the relation between them was also analyzed.

The present work analyses the coding efficiency of (1) Real-Imaginary versus Amplitude-Phase representation; (2) Hologram versus Object plane; and for (3) Computer generated and experimental holographic data.

2. Database

2.1. Optical recording

The evaluated digital holograms were acquired using phase-shifting holography. The recording setup comprises a Mach–Zehnder type interferometer working in the reflection mode and using an in-line configuration (see Fig. 1). According to this setup, a laser beam, produced by

[1] http://emergimg.di.ubi.pt.

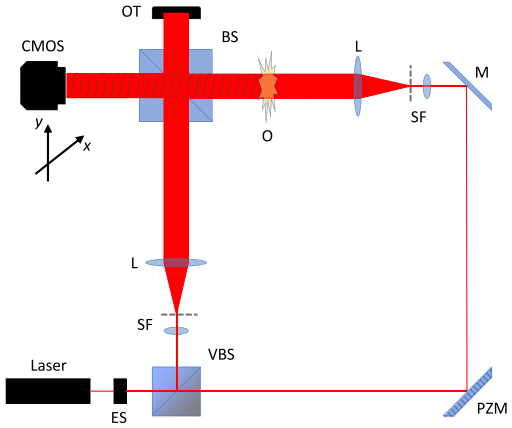

Fig. 1. Digital holography transmission setup based on the Mach–Zehnder interferometer. The laser beam goes through an electronic shutter (ES) and is then split into the reference and the object (O) arms by a variable beam splitter (VBS). Two spatial filters (SF) and collimating lenses (L) are used before combining both beams with a second beam splitter (BS), where an optical trap (OT) is added to suppress the transmitted part of the reference beam. A piezo-electric mirror (PZM), followed by the mirror (M), adjusts the phase between the two beams. A CMOS camera records the interference pattern.

a randomly polarized HeNe laser with 5 mW and 632.8 nm wavelength, is divided into a reference and an object beams by means of a variable beam splitter. The light reflected by the object is then combined with the reference beam, using a second beam splitter. The resultant interference pattern is digitized by a Guppy Pro F-503 camera having a CMOS sensor with a 4.4 μm × 4.4 μm effective pitch size, using an acquisition mode with 1296 × 972 pixels of resolution and 8 bit-depth. Each hologram is a combination of four phase-shifted interference patterns that are sequentially recorded, with a constant phase step of $\pi/2$, adjusted by a computer controlled piezo-electric mirror.

Several sequences of four phase-shifted interference patterns were acquired at "Universidade da Beira Interior" and can be found in the EmergImg-HoloGrail database. These include two chess pieces, a *Horse* and a *King*, a dice *Cube* and a sequence of 54 images of a rotating *Car*. An example of a set of four phase-shifted interference patterns for the *Horse* piece is presented in Fig. 2.

2.2. Phase shifting

Digital holography employs diffraction theory to recover the complex object field in a process called numerical reconstruction. According to this theory, the transmission of a reference beam through the digital hologram is simulated. The intensity of a digitally recorded hologram contains the image of an object, the conjugate image, and two zero-order images, according to the following expression:

$$I = |E_O + E_R|^2 = |E_O|^2 + |E_R|^2 + E_O E_R^\star + E_O^\star E_R, \tag{1}$$

where, $E_O E_R^\star$ is the object image, $E_O^\star E_R$ is the conjugate image, and $|E_O|^2$ and $|E_R|^2$ are the zero-order images. In order to retrieve the complex object field $E_O(x_0, y_0)$ at the recording plane and remove the zero order and the conjugate components, four holograms I_{α_i}, acquired sequentially with reference phases α_i separated by $\pi/2$ steps, are combined:

$$E_O = \frac{(I_0 - I_\pi) - j(I_{\pi/2} - I_{3\pi/2})}{4E_R^\star}, \tag{2}$$

where, the conjugate of the reference wave $E_R^\star$ is usually taken as unity when a plane wave reference beam is used.

The phase shifting results for each of the experimentally acquired holograms are available for download in the presented EmergImg-HoloGrail database.

2.3. Numerical reconstruction

The diffracted field $E_O(x, y; z)$, at a distance z from the hologram, can be written as:

$$E_O(x, y; z) = E_O(x_0, y_0) * h(x, y; z), \tag{3}$$

where, the symbol $*$ denotes the convolution operator and $h(x, y; z)$ is the free space Point Spread Function (PSF). The Eq. (3) entails the Huygens–Fresnel principle which, according to the paraxial approximation ($z^2 \gg x^2 + y^2$), gives the following PSF:

$$h(x, y; z) \approx \frac{e^{j2\pi z/\lambda}}{j\lambda z} e^{j\pi \frac{x^2+y^2}{\lambda z}}, \tag{4}$$

where, λ is the wavelength of light.

By replacing (4) into (3), we have,

$$E_O(x, y; z) = \frac{e^{j2\pi z/\lambda}}{j\lambda z} e^{j\pi \frac{x^2+y^2}{\lambda z}} \mathcal{F}\left\{ E_0(x_0, y_0)\, e^{j\pi \frac{x_0^2+y_0^2}{\lambda z}} \right\}, \tag{5}$$

where, the Fourier Transform has been defined with the new spatial frequencies $f_x = x/\lambda z$ and $f_y = y/\lambda z$. The method described by Eq. (5) is usually known as the Fresnel Transform Method.

The reconstruction function following the previous method is also available for download in EmergImg-HoloGrail database. The images shown in Fig. 4 were obtained applying this reconstruction method to the above mentioned experimental holograms, namely the *Horse*, the *King*, the *Cube*, and an example of the rotating *Car* sequence, using the parameters given in Table 1.

3. Method of analysis

The goal of the present work is to analyze the impact of codification in each propagation plane, hologram or object planes (see Fig. 3) for the different complex representation formats, namely Amplitude-Phase or Real-Imaginary, using experimental holograms and CGHs. This section presents the used data, the considered representations, the coding scheme, and finally the quality assessment methodology.

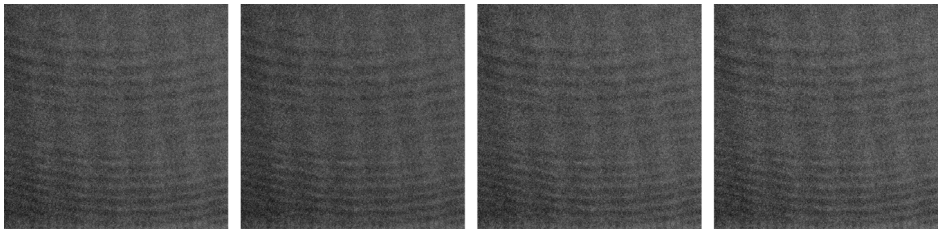

(a) 0 (b) $\frac{\pi}{2}$ (c) π (d) $\frac{3\pi}{2}$

Fig. 2. An example of the 4 interference patterns with 4 different phase-shifts for the *Horse* hologram.

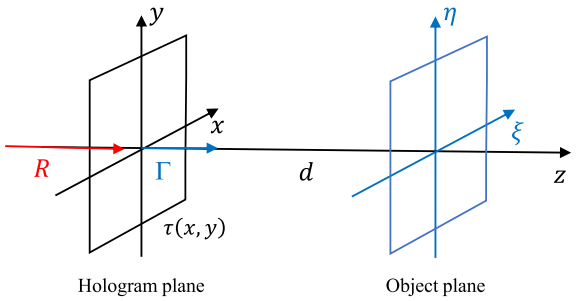

Fig. 3. Numerical holograms reconstruction: coordinate system.

3.1. Used data

In this work, four experimental holograms and eight CGHs were used. The experimental holograms were acquired with the optical recording setup presented in Fig. 1. The corresponding reconstructed amplitudes are represented in Fig. 4. All reconstructions have their speckle noise reduced by NonLocal Means filter [49].

Holograms can also be created by computer simulation of the light propagation, bypassing the need for an optical recording setup. The eight CGHs represented in Figs. 5 and 6 were selected from Interfere-I and Interfere-II databases, respectively [50].

The characteristics of each of the above mentioned holograms are presented in Table 1.

3.2. Data representation

Like in previous studies [44,50], two different holographic representation formats were considered in this work, the Real-Imaginary and Amplitude-Phase. Previous results with Phase Shifted Distances representation were very similar to the results obtained for the Real-Imaginary representation. Consequently, only the latter ones will be reported.

These representation formats were already used in previous works, but only in the hologram plane. In the object plane, only the amplitude of the reconstructed object is usually considered, since it is the one that provides a standard representation of the object. Since phase information is discarded, only a particular view, and a specific focusing distance, is represented in each frame. This excludes the reconstruction of other object configurations without requiring the original hologram. However, the possibility of coding the entire reconstructed complex field in the object plane (see Fig. 3) is explored in this work as in [27], where complex amplitudes are considered. This representation preserves the 3D nature of the holographic technique, enabling the return to the hologram plane or to alternative propagation planes for refocusing or multi-view purposes.

The Real-Imaginary and Amplitude-Phase representations were used to express the complex values either in the hologram plane, or in the object plane obtained after reconstruction.

3.3. Coding in hologram plane vs. object plane

According to Peixeiro et al. [44], the HEVC intra main coding profile proved to provide the best standardized codec performance for holographic data. Thus, in this work, the HEVC intra main coding profile is used for compression of the different representations, in both propagation planes. The higher input bitrate allowed in this profile is 16 bits. This is the only case of the "intra main rext" [51] that correspond to an extension of the intra coding profile. In this work, this extension was considered. Coding with 16 bits instead of 8 bits, allows a more precise propagation between planes with a slight difference in the PSNR vs bit rate as can be seen in Fig. 7 for the case of the CGH *3D Multi*. Considering for instance Interfere I, the error associated with this process is of order 6E−7 for 8 bits and 6E−12 for 16 bits respectively.

The steps involved in the coding and assessment tasks are represented in Figs. 8 and 9, when coding is performed either at the hologram plane or the object plane, respectively.

The values of amplitude (A), phase (P), real (R), and imaginary (I) are extracted from the Complex Hologram Field (U1), for compression at the hologram plane. The A, P, R, and I values are extracted from the Complex Object Field (U2) for compression at the object plane. The different A, P, R, and I values are all compressed independently.

The A, P, R, and I values, were converted into 16 bits integer format, as defined by the HEVC intra main coding profile, for different Quantization Parameters (QP), notably 37, 32, 27, 25, 23, 22, 19, 17, and 12, in both propagation planes.

The coded A and P values for all possible QPs combinations were used to obtain different coded complex fields. The same was performed for the coded R and I values. The Complex Hologram Field (U1) and Complex Object Field (U2), from the two representations, before and after coding were assessed as described in Section 3.4. Moreover, in case of hologram plane coding, numerical reconstruction of the complex object field from the complex hologram field for the two representations, before and after coding is also assessed, as represented in Fig. 8. Furthermore, in case of object plane coding, numerical reconstruction of the complex hologram field from the complex object field for the two

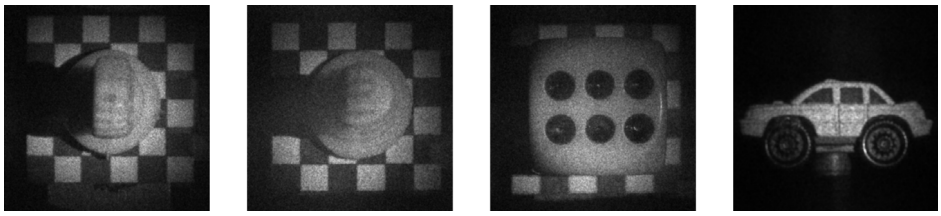

(a) *Horse* (b) *King* (c) *Cube* (d) *Car2575*

Fig. 4. Experimental acquired holograms.

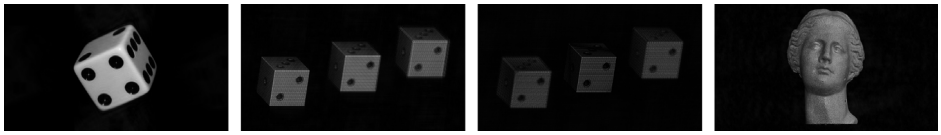

(a) *2D Dice* (b) *2D Multi* (c) *3D Multi* (d) *3D Venus*

Fig. 5. Synthetic holograms selected from Interfere-I database [50].

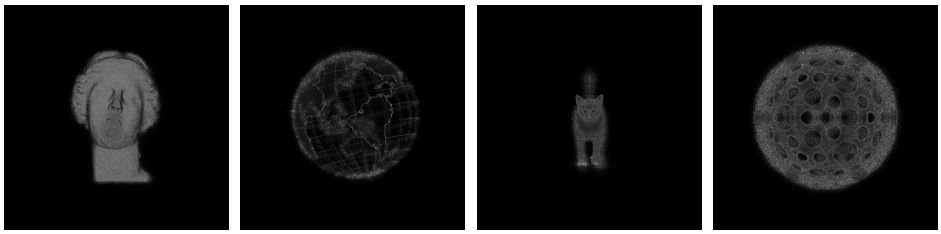

(a) *Venus8KS* (b) *Earth8KS* (c) *Cat8KS* (d) *Ball8KS*

Fig. 6. Synthetic holograms selected from Interfere-II database [50].

Table 1
Hologram characteristics.

	Resolution (pixel)	Pixel pitch (μm)	Reconstruction distance (m)	Wavelength (nm)
Horse	972 × 972	4.4	0.14	632.8
King	972 × 972	4.4	0.14	632.8
Cube	972 × 972	4.4	0.135	632.8
Car2575	600 × 600	4.4	0.245	632.8
2D Dice	1920 × 1080	8	0.90	632.8
2D Multi	1920 × 1080	8	0.50	632.8
3D Multi	1920 × 1080	8	0.50	632.8
3D Venus	1920 × 1080	8	0.50	632.8
Venus8KS	8192 × 8192	1	0.0129	633
Earth8KS	8192 × 8192	1	0.0118	633
Cat8KS	8192 × 8192	1	0.0142	633
Ball8KS	8192 × 8192	1	0.0125	633

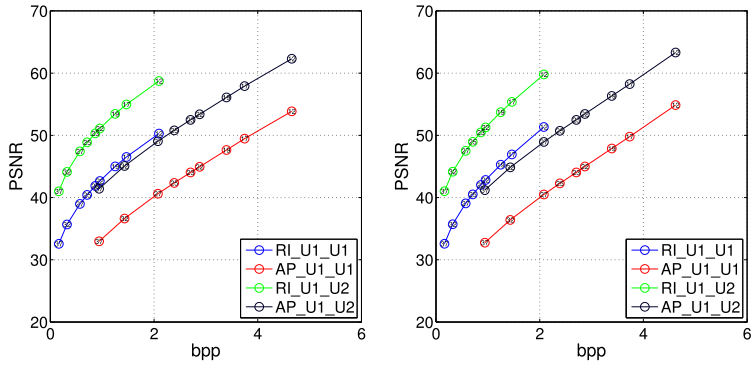

(a) Coding at hologram plane.

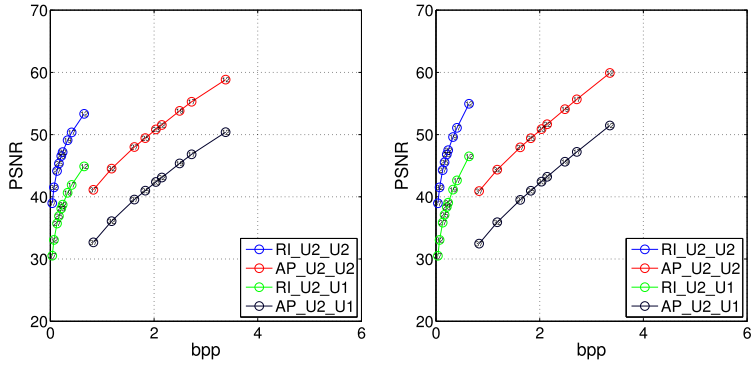

(b) Coding at object plane.

Fig. 7. Comparison between 8 and 16 bits for CGH *3D Multi*. Left — 8 bits; Right — 16 bits.

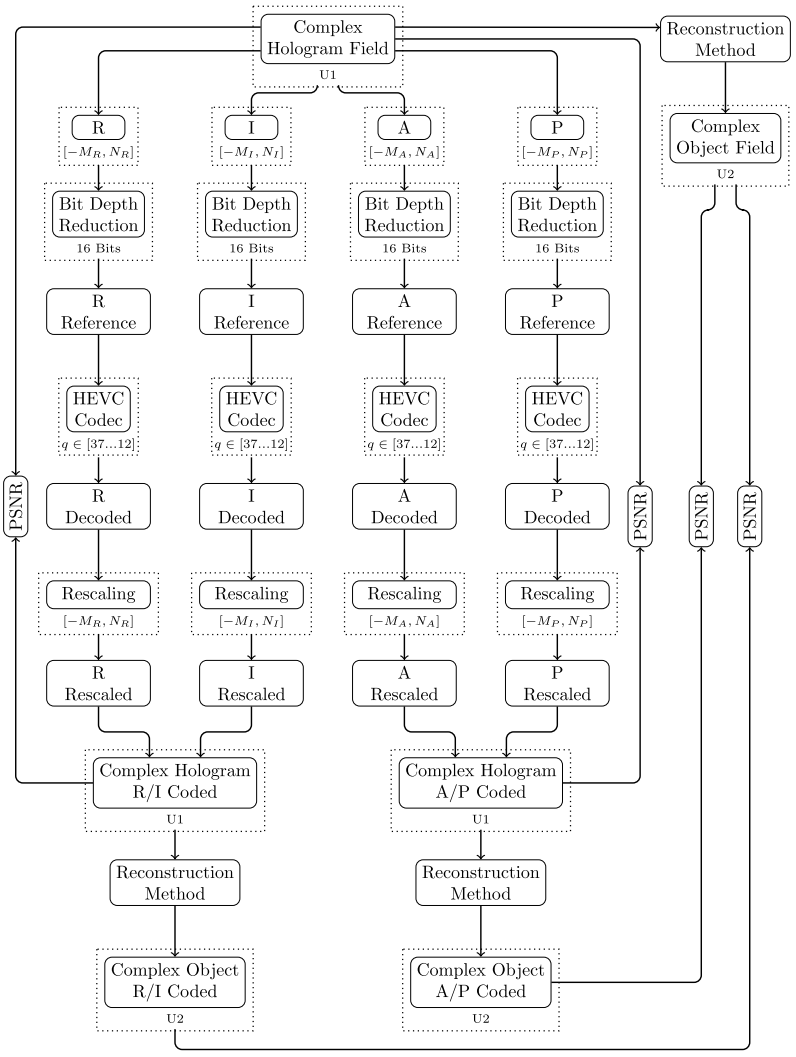

Fig. 8. Hologram plane coding and assessment scheme.: A — Amplitude; P — Phase; R — Real; I — Imaginary.

representations, before and after coding is also assessed, as represented in Fig. 9. It is important to clarify that the assessment is computed always considering the original image prior to any quantization.

3.4. Quality assessment

When considering holographic data, there are no standard metrics for the compression scheme's efficiency evaluation. Some metrics used on natural images, such as compression ratio, Normalized Root-Mean-Square (NRMS), or Peak Signal-To-Noise Ratio (PSNR) have been applied to either the compressed holograms or reconstructed images.

In this work, the performance is simultaneously assessed on the complex field in both holographic and object planes. The PSNR is applied to measure the quality as in standard images. Furthermore, the PSNR of the complex field is the mean of the PSNR values obtained for the real and imaginary parts (see Figs. 8 and 9).

The Bjontegaard delta peak-signal-to-noise ratio (BD-PSNR) and the Bjontegaard delta rate (BD-Rate) metrics [52] were also used to assess and compare the coding efficiency of both planes, notably hologram and object plane. The Bjontegaard model is used to calculate the average PSNR and bitrate differences between two R–D curves obtained from the PSNR measurement when encoding a content at different bitrates. The model reports two values, the BD-PSNR, which corresponds to the average PSNR difference in dB for the same bitrate, and the BD-Rate, which corresponds to the average bitrate difference in percent for the same PSNR.

4. Results and global analyses

In this section, the results obtained for the impact of HEVC in each Amplitude-Phase and Real-Imaginary representations, on the hologram and on the object plane in experimental holograms and CGHs are analyzed.

Figs. 10, 11, and 12 represent the bpp/PSNR relations for CGHs from Interfere-I, Interfere-II, and experimental holograms, respectively. All the relations are presented, namely, the two coding planes and the two assessment planes possibilities. More specifically, both Real-Imaginary (RI) and Amplitude-Phase (AP) representations are considered when coded at hologram (RI_U1 and AP_U1) and object (RI_U2 and AP_U2) planes. The assessment is also always performed in both planes, hologram plane (RI_U1_U1, AP_U1_U1, RI_U2_U1, and AP_U2_U1) and object plane (RI_U1_U2, AP_U1_U2, RI_U2_U2, and AP_U2_U2).

As already verified in the existing literature, the AP representation always presents much higher bitrates than RI representation. This is mainly due to the higher bitrate required for the Phase (P) compression. That reveals that the HEVC intra main coding profile is not appropriate to compress phase information, which is expected considering the specific type of information represented by the Holograms Phase.

Experimental holograms (Fig. 12) present higher bitrates than CGHs (Figs. 10 and 11). This is verified for both representations, but it is more evident for the RI representation. These results were expected since experimental holograms are affected by speckle noise, which obviously have a negative compression impact.

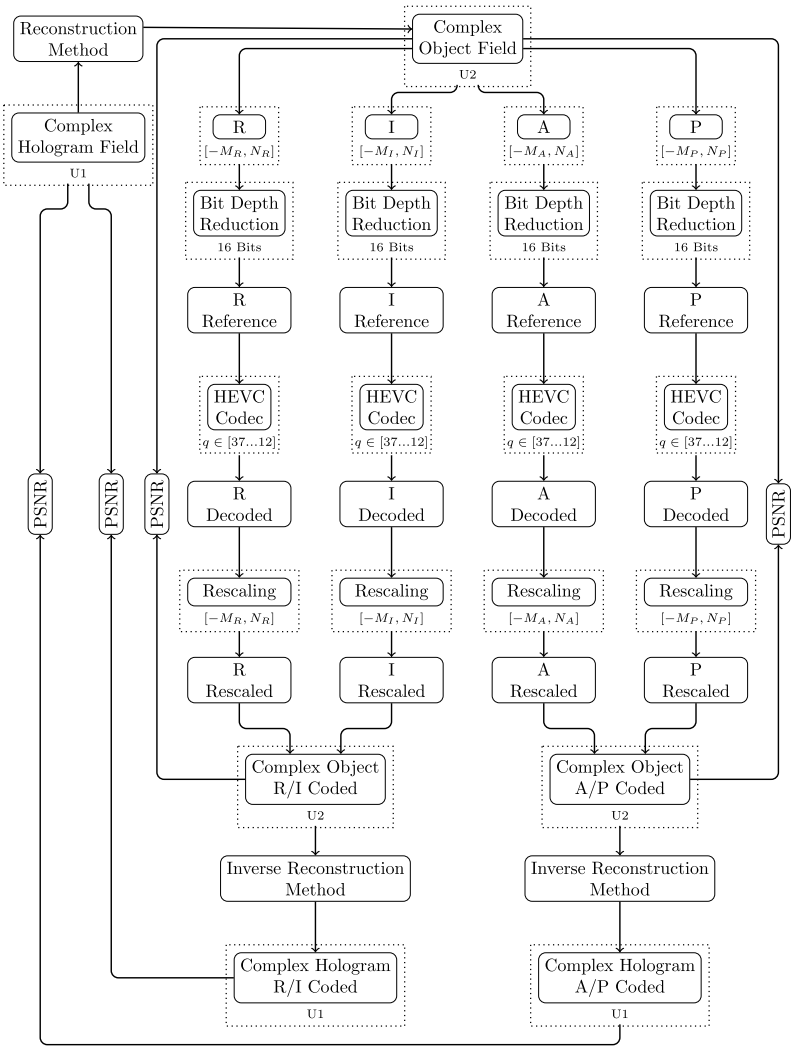

Fig. 9. Object plane coding and assessment scheme.: A — Amplitude; P — Phase; R — Real; I — Imaginary.

Comparing the two CGH databases, can be observed that for holograms from Interfere-II much lower bitrates are obtained, for both RI and AP representations.

In case of RI representation, when encoding is performed in the object plane the bitrates are always lower than when coding is performed in the hologram plane. These differences are more relevant for CGHs.

In case of AP representation the results are different for the three databases. In the case of database from Interfere-I, Fig. 10, a better performance is obtained when encoding the object plane. The CGH *2D Dice* results in an exception that can be explained by the reduced phase information of this specific hologram in the hologram plane. In the case of the Interfere-II database, Fig. 11, there are no differences between coding in hologram or object planes for *Venus8KS* and for *Ball8KS*. A better performance for encoding at hologram plane is achieved for *Earth8KS* and for *Cat8KS*. However, both codings, on hologram or on object planes, always result in high PSNRs (higher than 40 dB). For experimental holograms, Fig. 12, the differences of encoding on hologram or on object plane are minor.

Comparing the assessment on hologram plane (left columns of Figs. 10, 11, and 12) or on object plane (right columns of Figs. 10, 11, and 12) can be observed that results are similar, although a slightly better performance is obtained for the object plane. These results show that a very high correlation exists between results obtained in the hologram and object planes for the bpp/PSNR relation. Hence, assessment can be performed in any of the representation planes.

The results obtained with the Bjontegaard metrics when assessment is performed in hologram plane are presented in Tables 2, 3, and 4 for Interfere-I and Interfere-II CGHs, and experimental holograms, respectively. Similar tables, when assessment is performed in object plane are presented in Tables 5, 6, and 7.

The Bjontegaard metrics are used to verify the bitrate and PSNR gain for object plane encoding in relation to the hologram plane encoding. This analysis is performed for both representation formats and propagation planes. Comparing the two groups of tables confirms the similarity of assessment in the hologram and object planes. Moreover, can also be confirmed that the object plane compression provides the best option for RI representation format. The results for Interfere-I CGHs, Tables 2 and 5, and Interfere-II CGHs, Tables 3 and 6, are similar and seem to depend more on the content than on the different hologram characteristics.

The gain for experimental holograms is lower than the gain for CGHs. That can be partially explained by the speckle noise that has a greater impact on the experimental holograms. This was already noticed with the bpp/PSNR relation (Figs. 10, 11, and 12), where the experimental holograms present higher bitrates than the CGHs, for both representations. However, there may be other factors affecting the observed differences, namely, the numerical reconstruction methods, the recording parameters such as distance and pixel size, as well as the depth contents and sparse nature of each object scene. For example, it can be noted that the *car2575* has the highest BD-Rate among the

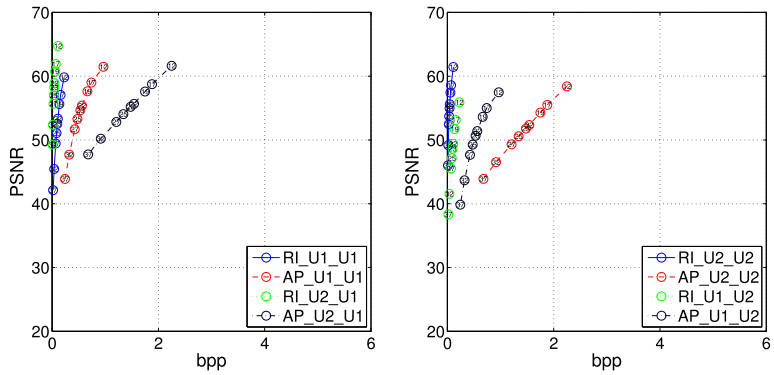

(a) Coding of *2D Dice* hologram.

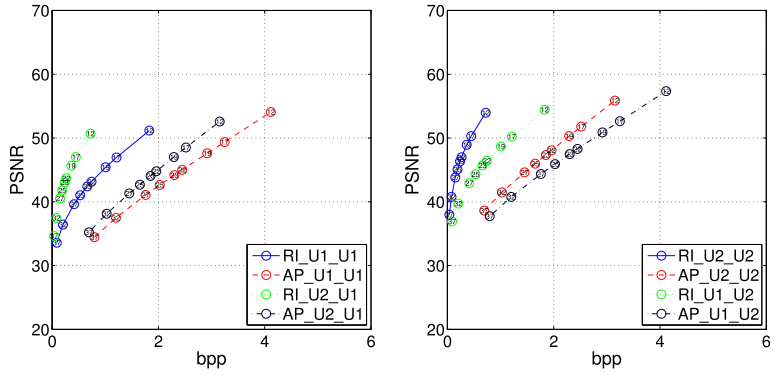

(b) Coding of *2D Multi* hologram.

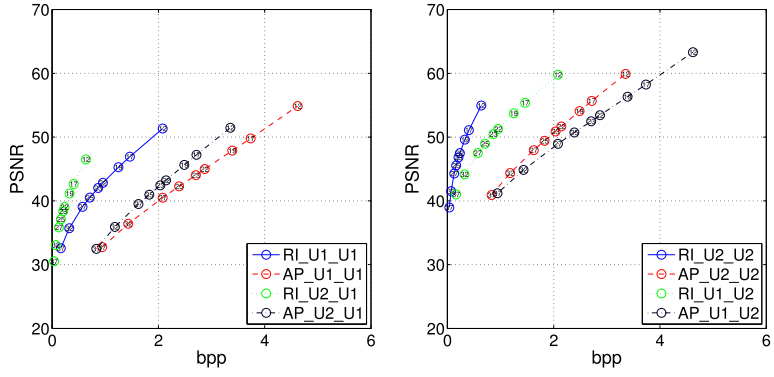

(c) Coding of *3D Multi* hologram.

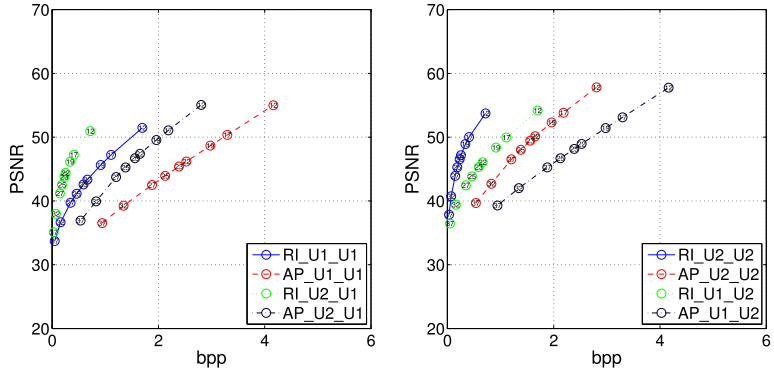

(d) Coding of *3D Venus* hologram.

Fig. 10. Coding of CGHs from Interfere-I. Left: assessed at hologram plane; Right: assessed at object plane.

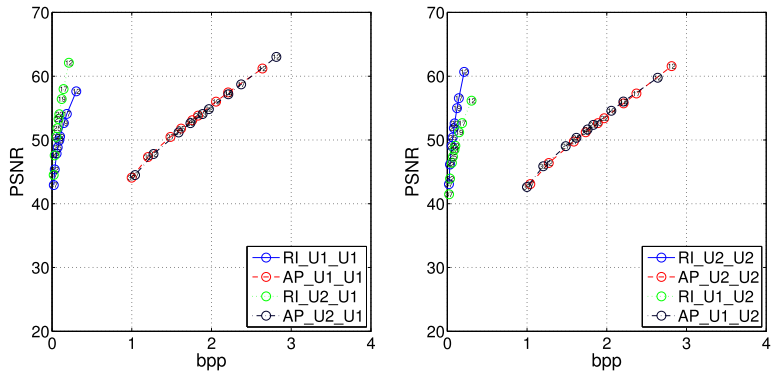

(a) Coding of *Venus8KS* hologram.

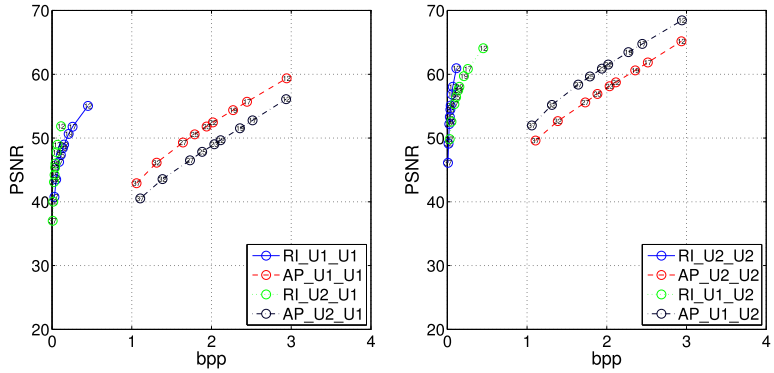

(b) Coding of *Earth8KS* hologram.

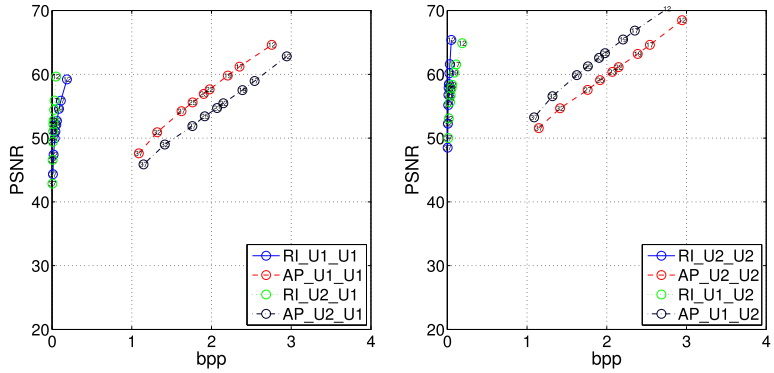

(c) Coding of *Cat8KS* hologram.

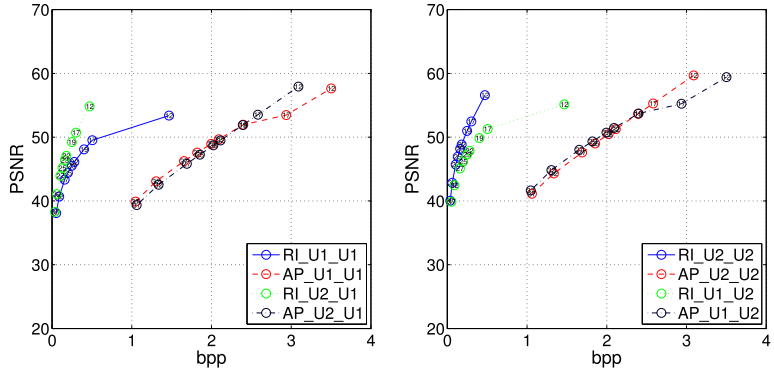

(d) Coding of *Ball8KS* hologram.

Fig. 11. Coding of CGHs from Interfere-II. Left: assessed at hologram plane; Right: assessed at object plane.

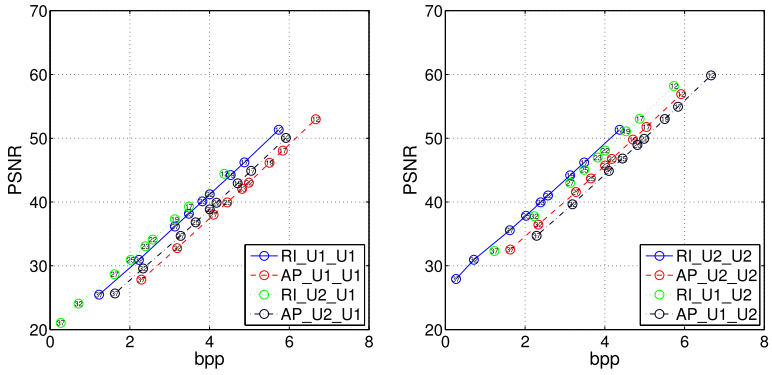

(a) Coding of *Horse* hologram.

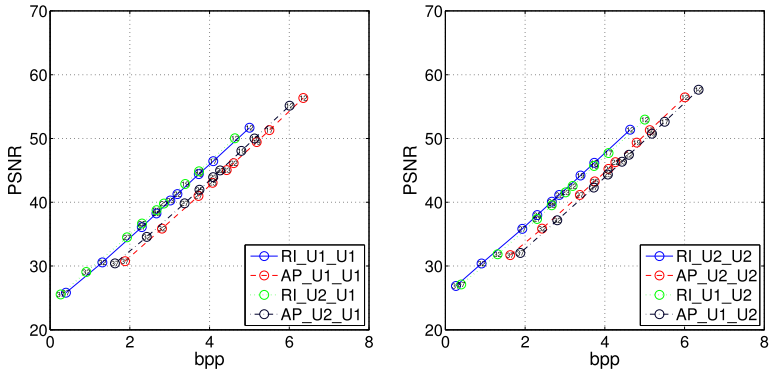

(b) Coding of *King* hologram.

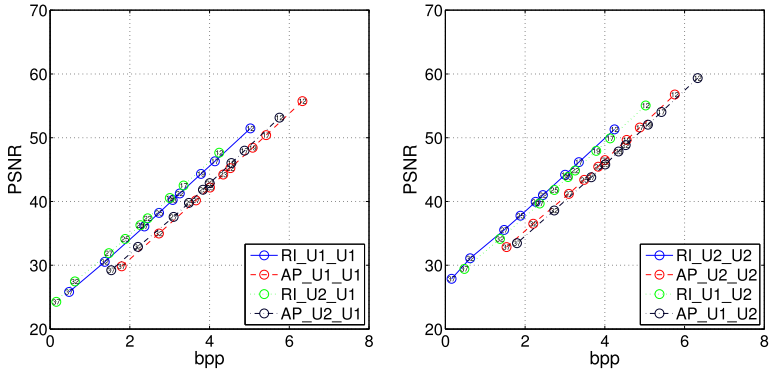

(c) Coding of *Cube* hologram.

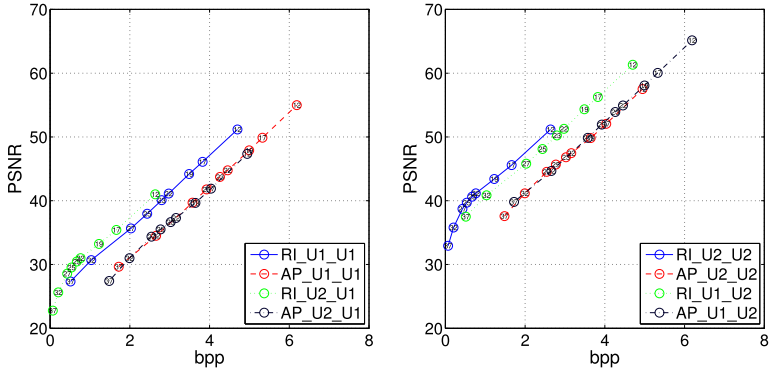

(d) Coding of *Car2575* hologram.

Fig. 12. Coding of experimental acquired holograms. Left: assessed at hologram plane; Right: assessed at object plane.

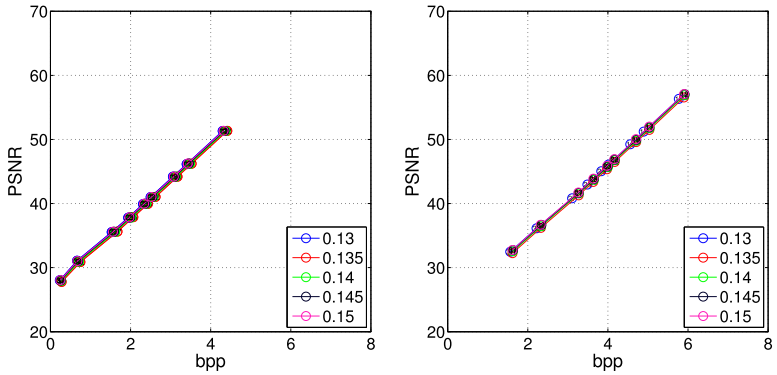

(a) Coding of *Horse* hologram.

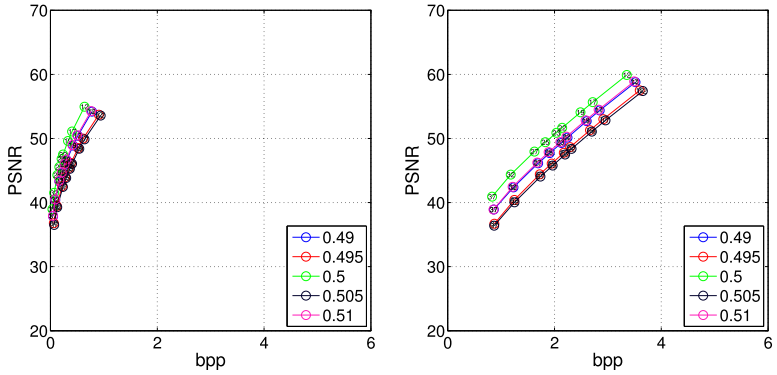

(b) Coding of *3D Multi* hologram.

Fig. 13. Coding considering different reconstruction distances. Left: RI representation; Right: AP representation.

Table 2
Bjontegaard metric for Interfere-I CGHs coded with HEVC, assessed in hologram plane. Average coding efficiency for object plane over hologram plane.

	2D Dice		*2D Multi*		*3D Multi*		*3D Venus*	
	BD-PSNR [dB]	BD-Rate [%]	BD-PSNR [dB]	BD-Rate [%]	BD-PSNR [dB]	BD-Rate [%]	BD-PSNR [dB]	BD-Rate [%]
RI	12.13	−81.45	6.08	−66.74	5.78	−58.60	5.25	−65.92
AP	−10.68	150.95	2.40	−19.20	2.09	−15.07	6.09	−40.23

Table 3
Bjontegaard metric for Interfere-II CGHs coded with HEVC, assessed in hologram plane. Average coding efficiency for object plane over hologram plane.

	Venus8KS		*Earth8KS*		*Cat8KS*		*Ball8KS*	
	BD-PSNR [dB]	BD-Rate [%]	BD-PSNR [dB]	BD-Rate [%]	BD-PSNR [dB]	BD-Rate [%]	BD-PSNR [dB]	BD-Rate [%]
RI	3.84	−46.19	3.81	−51.03	6.02	−66.83	3.29	−47.65
AP	−0.27	1.61	−3.40	24.37	−3.45	21.46	−0.12	−0.21

Table 4
Bjontegaard metric for experimental holograms coded with HEVC, assessed in hologram plane. Average coding efficiency for object plane over hologram plane.

	Horse		*King*		*Cube*		*Car2575*	
	BD-PSNR [dB]	BD-Rate [%]	BD-PSNR [dB]	BD-Rate [%]	BD-PSNR [dB]	BD-Rate [%]	BD-PSNR [dB]	BD-Rate [%]
RI	1.13	−8.83	0.54	−5.85	0.71	−9.21	1.85	−21.53
AP	1.47	−6.67	0.83	−4.24	0.70	−3.60	−0.03	0.98

Table 5
Bjontegaard metric for Interfere-I CGHs coded with HEVC, assessed in object plane. Average coding efficiency for object plane over hologram plane.

	2D Dice		*2D Multi*		*3D Multi*		*3D Venus*	
	BD-PSNR [dB]	BD-Rate [%]	BD-PSNR [dB]	BD-Rate [%]	BD-PSNR [dB]	BD-Rate [%]	BD-PSNR [dB]	BD-Rate [%]
RI	12.74	−83.09	6.06	−66.76	5.78	−58.60	5.27	−66.07
AP	−10.43	141.01	2.43	−19.46	2.09	−15.07	6.10	−40.25

experimental holograms, which can be due to its sparse nature in the spatial domain when compared to the other experimental cases.

The reconstruction distance is another factor that can be expected to play an important role in compression performance mostly in object

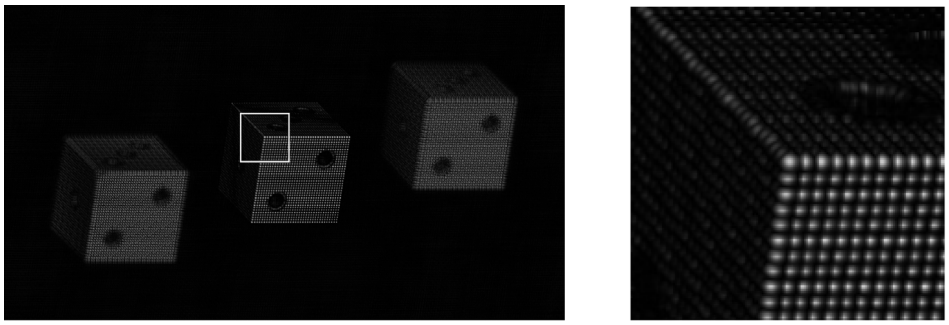

(a) Not compressed.

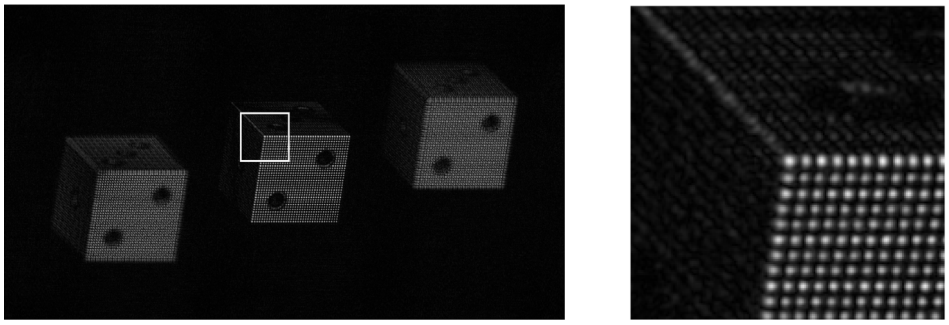

(b) Coded at hologram plane with a bitrate of 0.297 bpp.

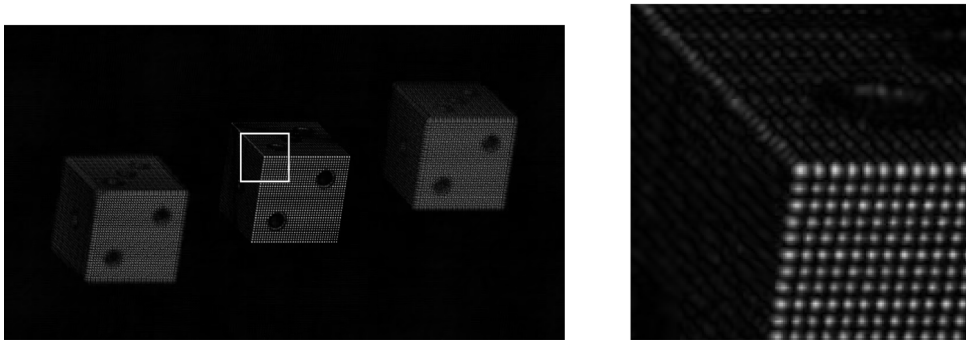

(c) Coded at object plane with a bitrate of 0.288 bpp.

Fig. 14. Left: Reconstructed amplitudes of *3D Multi* hologram; Right: Magnification of selected block in left image.

Table 6
Bjontegaard metric for Interfere-II CGHs coded with HEVC, assessed in object plane. Average coding efficiency for object plane over hologram plane.

	Venus8KS		*Earth8KS*		*Cat8KS*		*Ball8KS*	
	BD-PSNR [dB]	BD-Rate [%]	BD-PSNR [dB]	BD-Rate [%]	BD-PSNR [dB]	BD-Rate [%]	BD-PSNR [dB]	BD-Rate [%]
RI	3.84	−46.28	3.84	−51.29	6.07	−67.05	3.29	−47.66
AP	−0.25	1.49	−3.39	24.30	−3.43	21.35	−0.11	−0.26

Table 7
Bjontegaard metric for experimental holograms coded with HEVC, assessed in object plane. Average coding efficiency for object plane over hologram plane.

	Horse		*King*		*Cube*		*Car2575*	
	BD-PSNR [dB]	BD-Rate [%]	BD-PSNR [dB]	BD-Rate [%]	BD-PSNR [dB]	BD-Rate [%]	BD-PSNR [dB]	BD-Rate [%]
RI	1.17	−9.13	0.59	−6.32	0.77	−9.71	1.86	−21.67
AP	1.47	−6.67	0.83	−4.24	0.70	−3.60	−0.03	0.98

plane. The influence of this factor in object plane encoding is represented in Fig. 13 for a CGH and an experimental hologram. In case of experimental holograms the compression efficiency is only slightly affected by this parameter. In case of CGHs there is a larger influence of this parameter in compression efficiency. However, if this parameter is kept within the physical depth limits of the scene, the compression efficiency is still higher if performed in the object plane. Furthermore, the best reconstruction distance can be computed in case it is unknown, using an auto focus function [53–55].

Finally, some visual results are presented in Figs. 14 and 15. The reconstructed amplitudes of *3D Multi* hologram after coding in hologram and object plane for similar bitrates are presented in Fig. 14. It can be observed that the reconstructed object when coding was performed on object plane seems to be more focused (Comparing Fig. 14(b) and (c)).

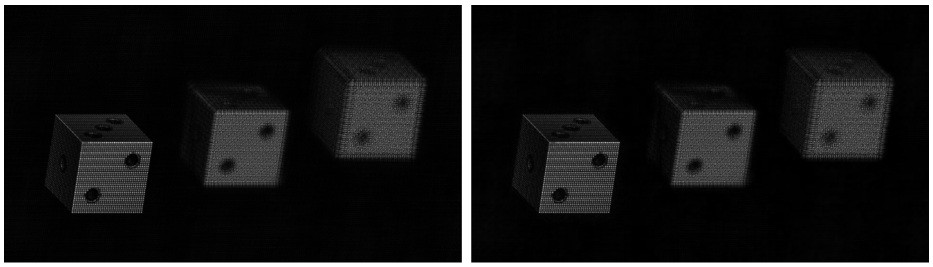

(a) Reconstructed amplitudes of *3D Multi* hologram, using reconstruction distance of 0.49 m.

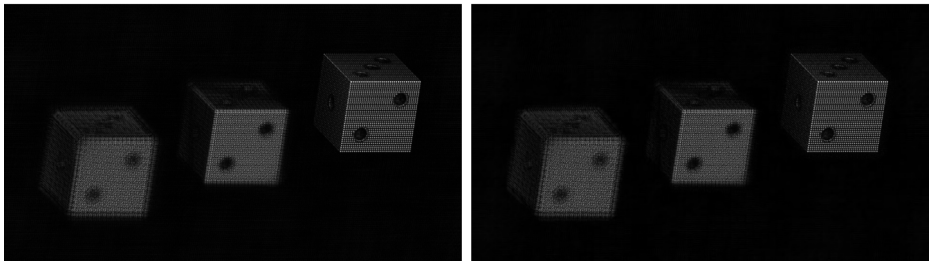

(b) Reconstructed amplitudes of *3D Multi* hologram, using reconstruction distance of 0.51 m.

Fig. 15. Left: Reference hologram; Right: Coded on object plane using reconstruction distance of 0.50 m, propagated to hologram plane, and reconstructed again with different distances.

For higher bitrates the visual differences with the original are difficult to perceive, independently of the coding plane.

The reconstructed amplitudes of *3D Multi* hologram considering reconstruction distance of 0.49 m and 0.51 m, after coding on object plane with a bitrate of 0.288 bpp and using reconstruction distance of 0.50 m are presented in Fig. 15. Once again, the visual differences with the original are difficult to perceive.

5. Conclusion

In this work, the coding performance of Amplitude-Phase and Real-Imaginary representations, on hologram and object propagation planes, for experimental holograms and CGHs, was analyzed. The assessment in both hologram and object planes is also studied.

The experimental holograms used in this work are made available in an open-access database. The optical recording, phase-shifting, and numerical reconstruction are detailed and the necessary MATLAB codes are also provided. The CGHs were selected from the open access Interfere-I and Interfere-II database [50].

In accordance with previous studies, the Real-Imaginary information is coded with higher efficiency than the Amplitude-Phase information.

This study also reveals that the object plane compression using HEVC intra main coding profile for experimental holograms and CGHs is a very efficient model that outperforms the compression on the hologram plane. This compression gain is more relevant in CGHs. The difference between experimental holograms and CGHs was somewhat expected since CGHs are less affected by speckle noise that is a characteristic of experimental holograms.

The conclusions above are very revealing because the amplitude in the object plane gives a direct 2D representation of the image. Hence, it might provide a two levels representation, using as first level any typical image coding mechanism, followed by a second level with the phase coding scheme that represents the associated 3D information. Eventually, if holographic displays are used, or other rendering applications such as depth map, extended depth of focus or multiple perspectives, a transformation from the object plane to another plane would be required. However, there are still advantages of coding on the object plane, because of the higher compression. The added transformation complexity is still very small when compared with the typical coding and display rendering computational complexity.

The results presented in this work are very encouraging since the possibility of encoding holographic information in the object plane becomes feasible and can be more convenient in a number of interesting applications. For instance, when dealing with experimental holograms, this can be a great advantage, since there are a large number of speckle reduction techniques that can be applied to the object plane, in contrast with the hologram plane. From the representation and compression point of view, this observation defines new paths of research and development.

Acknowledgments

The authors are very grateful to the Portuguese FCT-Fundação para a Ciência e Tecnologia and co-funded by FEDER-PT2020, Portugal partnership agreement under the project PTDC/EEI-PRO/2849/ 2014 - POCI-01-0145-FEDER-016693, and under the project UID/EEA/50008/ 2013.

References

[1] D. Gabor, et al., A new microscopic principle, Nature 161 (4098) (1948) 777–778.
[2] E. Leith, J. Upatnieks, Wavefront reconstruction with diffused illumination and threedimensional objects, J. Opt. Soc. Amer. 54 (11) (1964) 1295–1301.
[3] E. Leith, J. Upatnieks, Reconstructed wavefronts and communication theory, J. Opt. Soc. Amer. 52 (10) (1962) 1123–1130.
[4] Y.N. Denisyuk, Photographic reconstruction of the optical properties of an object in its own scattered radiation field, in: Soviet Physics Doklady, Vol. 7, 1962, p. 543.
[5] A.W. Lohmann, D.P. Paris, Binary fraunhofer holograms, generated by computer, Appl. Opt. 6 (10) (1967) 1739–1748.
[6] L. Yaroslavski, N. Merzlyakov, Methods of Digital Holography, Consultants Bureau, 1980.
[7] J.W. Goodman, R. Lawrence, Digital image formation from electronically detected holograms, Appl. Phys. Lett. 11 (3) (1967) 77–79.
[8] M. Kronrod, N. Merzlyakov, L. Yaroslavski, Reconstruction of holograms with a computer, Sov. Phys.-Tech. Phys. U.S.A. 17 (2) (1972) 333–334.
[9] G. Liu, P.D. Scott, Phase retrieval and twin-image elimination for in-line fresnel holograms, J. Opt. Soc. Am. A 4 (1) (1987) 159–165.
[10] L. Onural, M.T. Özgen, Extraction of three-dimensional object-location information directly from in-line holograms using wigner analysis, J. Opt. Soc. Am. A 9 (2) (1992) 252–260.

[11] U. Schnars, W. Jüptner, Direct recording of holograms by a ccd target and numerical reconstruction, Appl. Opt. 33 (2) (1994) 179–181.
[12] J.F. Heanue, M.C. Bashaw, L. Hesselink, Encrypted holographic data storage based on orthogonal-phase-code multiplexing, Appl. Opt. 34 (26) (1995) 6012–6015.
[13] K. Curtis, W. Wilson, L. Dhar, Commercialization of holographic storage at inphase technologies, in: International Symposium on Optical Memory and Optical Data Storage Topical Meeting, 2002, pp. 6–8. http://dx.doi.org/10.1109/OMODS.2002.1028549.
[14] H. Horimai, X. Tan, Holographic information storage system: today and future, IEEE Trans. Magn. 43 (2) (2007) 943–947.
[15] L. Ferri, A. Mayerhoefer, M. Frank, C. Vielhauer, R. Steinmetz, Biometric authentication for ID cards with hologram watermarks, Proc. SPIE 4675 (2002) 629.
[16] G. Spagnolo, C. Simonetti, L. Cozzella, Content fragile watermarking based on a computer generated hologram coding technique, J. Opt. A: Pure Appl. Opt. 7 (7) (2005) 333–342.
[17] W. Plesniak, M. Halle, S. Pieper, W. Wells, M. Jakab, D. Meier, S. Benton, R. Guttmann, R. Kikinis, Holographic video display of time-series volumetric medical data, in: Visualization, 2003. VIS 2003, IEEE, IEEE, 2003, pp. 589–596.
[18] F. Cheong, B. Dreyfus, J. Amato-Grill, K. Xiao, L. Dixon, D. Grier, Flow visualization and flow cytometry with holographic video microscopy, Opt. Express 17 (15) (2009) 13071–13079.
[19] Y. Sun, Application of digital holography in displacement measurement, in: 2nd International Congress on Image and Signal Processing, 2009, CISP'09, IEEE, 2009, pp. 1–5.
[20] L. Onural, F. Yaras, H. Kang, Digital holographic three-dimensional video displays, Proc. IEEE 99 (4) (2011) 576–589.
[21] F. Yaras, H. Kang, L. Onural, State of the art in holographic displays: A survey, J. Disp. Technol. 6 (10) (2010) 443–454.
[22] K. Sato, K. Higuchi, H. Katsuma, Holographic television by liquid crystal device, in: Third International Conference on Holographic Systems, Components and Applications, 1991, IET, 1991, pp. 20–23.
[23] H. Yoshikawa, Digital holographic signal processing, in: Proceeding of the TAO First International Symposium, 1993, pp. S–4–2.
[24] H. Yoshikawa, J. Tamai, Holographic image compression by motion picture coding, in: Proceedings of SPIE, 2652, 1996, p. 2.
[25] J. Naughton, Y. Frauel, B. Javidi, E. Tajahuerce, Compression of digital holograms for three-dimensional object reconstruction and recognition, Appl. Opt. 41 (20) (2002) 4124–4132.
[26] G.A. Mills, I. Yamaguchi, Effects of quantization in phase-shifting digital holography, Appl. Opt. 44 (7) (2005) 1216–1225.
[27] E. Darakis, J.J. Soraghan, Reconstruction domain compression of phase-shifting digital holograms, Appl. Opt. 46 (3) (2007) 351–356.
[28] J. Naughton, B. McDonald, B. Javidi, Efficient compression of fresnel fields for internet transmission of three-dimensional images, Appl. Opt. 42 (23) (2003) 4758–4764.
[29] E. Darakis, J. Soraghan, Compression of interference patterns with application to phase-shifting digital holography, Appl. Opt. 45 (11) (2006) 2437–2443.
[30] E. Darakis, J. Soraghan, Use of fresnelets for phase-shifting digital hologram compression, IEEE Trans. Image Process. 15 (12) (2006) 3804–3811.
[31] M. Liebling, T. Blu, M. Unser, Fresnelets: new multiresolution wavelet bases for digital holography, IEEE Trans. Image Process.: Publ. IEEE Signal Process. Soc. 12 (1) (2003) 29–43.
[32] Y. Frauel, T.J. Naughton, O. Matoba, E. Tajahuerce, B. Javidi, Three-dimensional imaging and processing using computational holographic imaging, in: Proceedings of IEEE, Special Issue on 3-D Technologies for Imaging Display, Vol. 94, 2006, p. 636.
[33] Y. Seo, H. Choi, J. Bae, J. Yoo, D. Kim, Data compression technique for digital holograms using a temporally scalable coding method for 2-D images, in: IEEE International Symposium on Signal Processing and Information Technology, 2006, pp. 326–331.
[34] Y. Seo, H. Choi, D. Kim, Lossy coding technique for digital holographic signal, Opt. Eng. 45 (6) (2006) 065802.
[35] Y. Seo, H. Choi, D. Kim, 3D scanning-based compression technique for digital hologram video, Image Commun. 22 (2) (2007) 144–156.
[36] E. Shortt, J. Naughton, B. Javidi, Histogram approaches for lossy compression of digital holograms of three-dimensional objects, IEEE Trans. Image Process. 16 (6) (2007) 1548–1556.
[37] E. Darakis, M. Kowiel, R. Nasanen, J. Naughton, Visually lossless compression of digital hologram sequences, in: SPIE Proceedings, Vol. 7529, 2010, pp. 752912–752912–8.
[38] A. Arrifano, M. Antonini, M. Pereira, Multiple description coding of digital holograms using maximum-a-posteriori, in: European Workshop on Visual Information Processing, 2013, pp. 232–237.
[39] D. Blinder, T. Bruylants, E. Stijns, H. Ottevaere, P. Schelkens, Wavelet coding of off-axis holographic images, in: Proc. SPIE, Vol. 8856, 2013, pp. 88561L–88561L–12.
[40] K. Viswanathan, P. Gioia, L. Morin, Morlet wavelet transformed holograms for numerical adaptive view-based reconstruction, in: Proc. SPIE, Vol. 9216, 2014, pp. 92160G–92160G–14.
[41] Y. Xing, M. Kaaniche, B. Pesquet-Popescu, F. Dufaux, Adaptive nonseparable vector lifting scheme for digital holographic data compression, Appl. Opt. 54 (1) (2015) A98–A109.
[42] Y. Xing, B. Pesquet-Popescu, F. Dufaux, Comparative study of scalar and vector quantization on different phase-shifting digital holographic data representations, in: 3DTV-Conference, Budapest. Hungry, 2014.
[43] Y. Xing, M. Kaaniche, B. Pesquet-Popescu, F. Dufaux, Vector lifting scheme for phase-shifting holographic data compression, Opt. Eng. 53 (11) (2014) 112312–112312.
[44] J. Peixeiro, C. Brites, J. Ascenso, F. Pereira, Digital holography: Benchmarking coding standards and representation formats, in: IEEE International Conf. on Multimedia and Expo - ICME, 2016.
[45] F. Dufaux, Y. Xing, B. Pesquet-Popescu, P. Schelkens, Compression of digital holographic data: an overview, Proc. SPIE 9599 (2015) 95990I–95990I–11.
[46] Y. Xing, M. Kaaniche, B. Pesquet-Popescu, F. Dufaux (Eds.), Digital Holographic Data Representation and Compression, Academic Press, 2016.
[47] I. Yamaguchi, T. Zhang, Phase-shifting digital holography, Opt. Lett. 22 (16) (1997) 1268–1270.
[48] M. Bernardo, A. Pinheiro, M. Pereira, Benchmarking coding standards for digital holography represented on the object plane, in: Proc. SPIE, Spie, 2018, pp. 6–8.
[49] A. Uzan, Y. Rivenson, A. Stern, Speckle denoising in digital holography by nonlocal means filtering, Appl. Opt. 52 (1) (2013) A195–A200.
[50] D. Blinder, A. Ahar, A. Symeonidou, Y. Xing, T. Bruylants, C. Schreites, B. Pesquet-Popescu, F. Dufaux, A. Munteanu, P. Schelkens, Open access database for experimental validations of holographic compression engines, in: Seventh International Workshop on Quality of Multimedia Experience, 2015, pp. 1–6.
[51] F.H.H. Institute, High Efficiency Video Coding (HEVC). URL https://hevc.hhi.fraunhofer.de.
[52] G. Bjontegaard, Improvements of the BD-PSNR model, in: ITU 35th Meeting VCEG.
[53] F.C. Groen, I.a.T. Young, G. Ligthart, A comparison of different focus functions for use in autofocus algorithms, Cytometry 6 (1985) 81–91.
[54] H. Mir, P. Xu, P.V. Beek, An extensive empirical evaluation of focus measures for digital photography, Proc. SPIE 9023 (2014) 90230I–90230I–11.
[55] E. Fonseca, P. Fiadeiro, M. Pereira, A. Pinheiro, Comparative analysis of autofocus functions in digital in-line phase-shifting holography, Appl. Opt. 55 (27) (2016) 7663–7674.